Optimizing core-shell nanoparticle catalysts with a genetic algorithm

Nathan S. Froemming and Graeme Henkelman[a)]
*Department of Chemistry and Biochemistry, The University of Texas at Austin,
Austin, Texas 78712-0165, USA*

A genetic algorithm is used with density functional theory to investigate the catalytic properties of 38- and 79-atom bimetallic core-shell nanoparticles for the oxygen reduction reaction. Each particle is represented by a two-gene chromosome that identifies its core and shell metals. The fitness of each particle is specified by how close the d-band level of the shell is to that of the Pt(111) surface, a catalyst known to be effective for oxygen reduction. The genetic algorithm starts by creating an initial population of random core-shell particles. The fittest particles are then bred and mutated to replace the least-fit particles in the population and form successive generations. The genetic algorithm iteratively refines the population of candidate catalysts more efficiently than Monte Carlo or random sampling, and we demonstrate how the average energy of the surface d-band can be tuned to that of Pt(111) by varying the core and shell metals. The binding of oxygen is a more direct measure of catalytic activity and is used to further investigate the fittest particles found by the genetic algorithm. The oxygen binding energy is found to vary linearly with the d-band level for particles with the same shell metal, but there is considerable variation in the trend across different shells. Several particles with oxygen binding energies similar to Pt(111) have already been investigated experimentally and found to be active for oxygen reduction. In this work, many other candidates are identified. © *2009 American Institute of Physics*. [doi:10.1063/1.3272274]

I. INTRODUCTION

Platinum-based fuel cells offer an attractive alternative to internal combustion engines as a future means of utilizing chemical energy. There are, however, shortcomings of such technologies that must be resolved if they are to become practical and widespread. Some of these difficulties include CO poisoning, the short lifetime of electrodes in acidic environments, the $\sim 30\%$ energy loss due to slow oxygen reduction kinetics, and the high material cost and limited supply of platinum itself. Cheaper, more effective electrocatalysts need to be developed, yet the task of discovering novel platinum alternatives has proven to be extremely challenging.

Nanoparticles have drawn considerable attention as potential catalysts. One reason is that nanoparticles have high surface-area-to-volume ratios, which could help reduce fuel cell cost since less catalytic material is required. Another reason is that nanoparticles can exhibit strikingly different reactivity than their bulk counterparts. Haruta *et al.*,[1,2] for example, have shown that supported Au particles are very active for low-temperature CO oxidation in the 2–5 nm size range. Bimetallic nanoparticles, moreover, offer the additional prospect of having their reactivity tuned as near-surface alloys.[3,4] Core-shell nanoparticles are excellent candidates because they have well-defined geometries when synthesized in controlled environments, for example, using dendrimer encapsulation techniques.[5,6]

In this work, we identify potential core-shell nanoparticle catalysts for the oxygen reduction reaction (ORR) using a genetic algorithm (GA) to search through the space of possible metal combinations. GAs have been used to solve complex problems in a wide variety of disciplines, including business,[7] bioinformatics,[8–10] chemistry,[11–13] data analysis,[14] economics and finance,[15–18] materials design,[19] and medicine.[20,21] They attempt to optimize an objective (fitness) function using biologically inspired analogs of selection, breeding, and mutation to iteratively refine a population of solution candidates. GAs are especially useful for systems involving discrete variables. In our case, the discreteness in the fitness landscape arises from the elemental identity of the core and shell metals; these are not continuous variables that can be optimized using gradient-based techniques. Our measure of a fit nanoparticle catalyst is that the center of the surface d-band is close to that of an effective catalyst, Pt(111). Studies have shown that the d-band is a good reactivity descriptor that can be used to predict trends in catalysts with similar geometries and reaction mechanisms.[4,22–24]

In order for GAs to be effective over random or trial-and-error sampling, there must be some structure to the fitness landscape. Two specific requirements are that (i) small mutations of a fit individual will tend to produce other fit individuals, and (ii) the properties that make two individuals fit can be encoded into their genetic information so that cross-breeding them will tend to produce other fit individuals. When these assumptions hold, the GA need only search through a small subset of the entire solution space to find the fittest individuals. We anticipate that the space of bimetallic core-shell nanoparticles is structured so that desirable particle properties can be optimized by a GA, i.e., that varying

a)Electronic mail: henkelman@mail.utexas.edu.

(a)   (b)
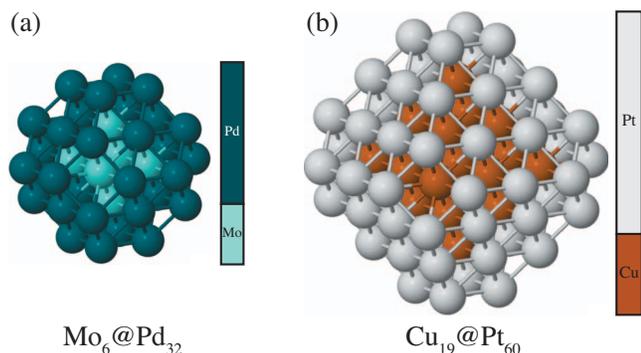
$Mo_6@Pd_{32}$ $Cu_{19}@Pt_{60}$

FIG. 1. Examples of the core-shell nanoparticles investigated in this work: (a) a 38-atom particle with a 6-atom molybdenum core and a 32-atom palladium shell, denoted $Mo_6@Pd_{32}$, and (b) a 79-atom $Cu_{19}@Pt_{60}$ particle. To the right of each nanoparticle is its two-gene chromosome.

the core of a particle with a good fitness value will tend to produce other fit particles and that the offspring of two fit particles will also tend to be fit.

II. CALCULATION DETAILS

Density functional theory (DFT) was used in a GA schema to optimize the identity of core and shell metals in 38- and 79-atom nanoparticle catalysts for the ORR. The particles were assumed to have face-centered cubic (fcc) crystal structures with the truncated-octahedral shapes shown in Fig. 1. The 38-atom particles contain a 6-atom core surrounded by a 32-atom monolayer shell, and the 79-atom particles contain a 19-atom core surrounded by a 60-atom monolayer shell. The cores and shells of the particles were taken to be *d*-block metals (viz., the chemical elements in groups 3–12 and periods 4–6 of the periodic table).

A flow chart of the GA used in this work is shown in Fig. 2. In the first step (a) an initial population of 30 core-shell nanoparticles was randomly generated using metals from the *d*-block. Each metal was used once as a core and once as a shell to ensure that a large region of solution space was initially sampled. The particles were given ideal fcc truncated-octahedral crystallite structures (Fig. 1) with the lattice constant chosen as a weighted average of the core and shell bulk fcc lattice constants.[25]

In the second step (b) DFT was used to optimize the structure of each particle in the generation and to calculate the electronic density of states. All DFT calculations were performed with the Vienna *ab initio* simulation package.[26,27] Geometry optimizations were initialized by randomly displacing each atom in the particle by a small amount (≤ 0.5 Å) to break symmetry. The total energy was then minimized until the force on each atom was less than 0.01 eV/Å. Cubic cells of side lengths 16 and 20 Å contained the 38- and 79-atom nanoparticles, respectively. These cell sizes were chosen so that 8 Å vacuum gap separated the periodic images on average. Electrons in the atomic cores were described using pseudopotentials of the projector augmented-wave framework,[28,29] while valence electrons were described with Kohn-Sham single-electron wave functions[30] expanded in a plane wave basis set up to a kinetic energy cutoff of 300 eV. The exchange-correlation potential was modeled with the

(a) **Start** by generating an initial population of random core-shell nanoparticles.

(b) **Evaluate** the electronic structure of each particle.

(c) **Rank** each nanoparticle using the fitness function,
$$\Phi \equiv \left| \varepsilon_d^{shell} - \varepsilon_d^{Pt(111)} \right|,$$
where ε_d^{shell} and $\varepsilon_d^{Pt(111)}$ are the *d*-band centers of the surface of the particle and Pt(111), respectively.

(d) **Breed** the nanoparticles according to the probability
$$P_{breed}(r) \propto e^{-\lambda r},$$
where r is the rank number. Alternatively, mutate a parent particle with 10% probability.

(e) **Finish** when the average fitness of the particles stops improving or is below a predefined threshold.

Create generation $N+1$

FIG. 2. Overview of the GA (see text for details). The steps in red were repeated to refine the population of candidate nanoparticle catalysts until the stop criterion was met.

generalized gradient approximation using the Perdew–Wang 91 functional.[31] The Brillouin zone was sampled at the Γ-point. Spin polarization was incorporated into all calculations. To accelerate electronic minimization, the occupation of states near the Fermi level was smeared by a width of 0.2 eV using the approach of Methfessel and Paxton.[32] Convergence was checked by increasing the plane wave energy cutoff to 400 eV and increasing the cell volume by 33%; the binding energy of oxygen on Ni_{79} changed by only 11 meV, or less than 0.4%, using these parameters. The symmetry of the particles was monitored during structural optimization. Any particle that did not retain a truncated-octrahedral core-shell geometry was removed from the simulation.

In the third step of the GA [Fig. 2(c)] the fitness of each particle was calculated using the fitness function

$$\Phi \equiv \left| \epsilon_d^{shell} - \epsilon_d^{Pt(111)} \right|, \qquad (1)$$

where ϵ_d^{shell} and $\epsilon_d^{Pt(111)}$ are the average energies of the *d*-band states in the shell of the particle and at the surface of Pt(111), respectively, each with reference to the Fermi energy.[33] This fitness function aims to quantify the activity of the catalytic surface of the nanoparticle with reference to Pt(111), an effective catalyst for the ORR. Once Φ was computed for all nanoparticles in the generation, the particles were ranked in ascending order of Φ. The particle with the smallest value of Φ received the best rank ($r=1$), while the particle with the largest value of Φ received the worst rank ($r=30$, assuming that no nanoparticles were discarded from the generation due to loss of symmetry).

In the fourth step (d) the nanoparticles were bred to produce the next generation. Parent nanoparticles were selected pairwise from the ranked generation according to the probability
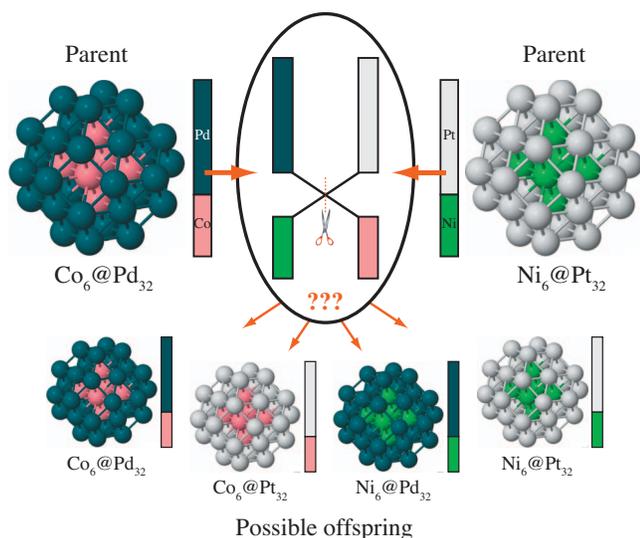
FIG. 3. Two parent particles are bred to produce an offspring particle. Each breeding event led to the formation of a single offspring, chosen at random from the set of possible offspring (in this case, $\{Co, Ni\}_6 @ \{Pd, Pt\}_{32}$).

$$P_{breed}(r) = \frac{e^{-\lambda r}}{\sum_{r'=1}^{R} e^{-\lambda r'}}, \qquad (2)$$

where $\lambda = \ln 10 / (R - 1)$ was chosen so that the breeding probability decreased by one decade over the size of the generation, R. The best-ranked particle was therefore 10 times more likely to breed than the worst-ranked particle, yet all particles were allowed to contribute to the next generation. Tests using different values of λ, chosen such that the breeding probability fell off by factors of 5 and 20, and using a step breeding probability function centered about $R/2$ (truncation) changed the number of fit particles found by the GA by less than 4%. This indicates that the performance of the GA is insensitive to the details of the breeding probability.

An example of the nanoparticle breeding process is shown in Fig. 3. A two-gene chromosome was used to identify the core and shell metals of each parent. The chromosomes of the parents were crossed to produce a single offspring nanoparticle for the next generation, chosen at random from the set of possible offspring. The breeding process was repeated until the next generation of 30 nanoparticles was formed. The 79-atom nanoparticles were bred in an identical manner.

Alternatively, parent nanoparticles had a chance to mutate. Mutations introduced randomness into the simulation and prevented the GA from becoming trapped in a local region of solution space. The mutations used in the GA are shown in Fig. 4. In a single-point mutation, either the core or the shell was mutated (with equal probability) to a random transition metal. In a double-point mutation both the core and the shell were mutated, corresponding to the formation of a new, random particle. In an inversion mutation, the core and shell metals were interchanged. The overall probability of a mutation occurring for a parent was 10%; the probability of a particular mutation was 3.3%.
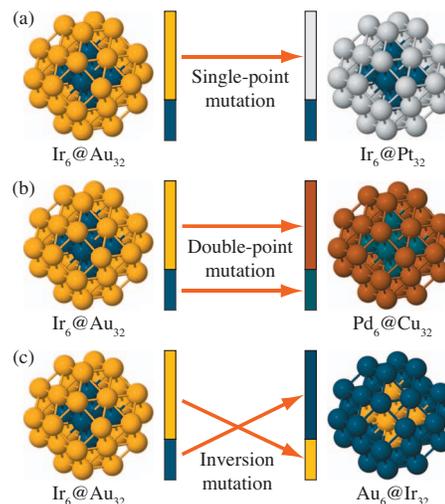
FIG. 4. Mutations used in the GA were (a) single-point, (b) double-point, and (c) inversion. For single-point mutations, either the core or the shell was mutated with equal probability. A mutation occurred with a probability of 10% during each breeding event.

Steps (b)–(d) in the GA were repeated to search for optimal core-shell nanoparticle catalysts. Each generation was evaluated with DFT, ranked, and bred to form the next generation; this generation in turn was evaluated with DFT, ranked and bred to form the next generation, and so on. In this way, the genes of fit particles propagated throughout the generations, and successive generations continually evolved toward optimal fitness. The GA was terminated once the average fitness of the generation dropped below 0.25 eV. Thus, the final generation had catalytic surfaces whose d-band centers were within 0.25 eV of Pt(111).

III. RESULTS AND DISCUSSION

A. 38-atom nanoparticles

Our first GA simulation optimized 38-atom core-shell particles for the ORR. Such particles may be too small to be stable as real catalysts, but they are well suited for testing our methodology. The convergence of the GA is shown in Fig. 5. The GA iteratively refined the population of candidate catalysts until the stop criterion $\Phi_{avg} \leq 0.25$ eV was reached.

Promising core-shell metal combinations found by the GA are shown in Fig. 6. Horizontal trends are prominent, indicating that the shell metal largely determines the electronic structure at the surface. Good shell metals include Cu, Mo, Os, Pd, Pt, and Ru. The presence of vertical trends in
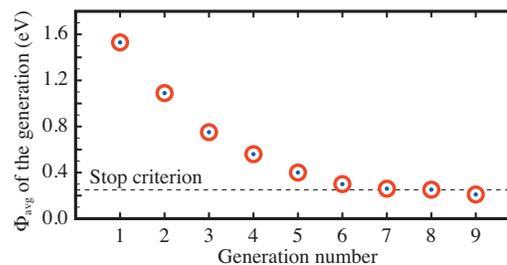
FIG. 5. Convergence of the GA for 38-atom particles. The average fitness of the generation decreased until the stop criterion was met.
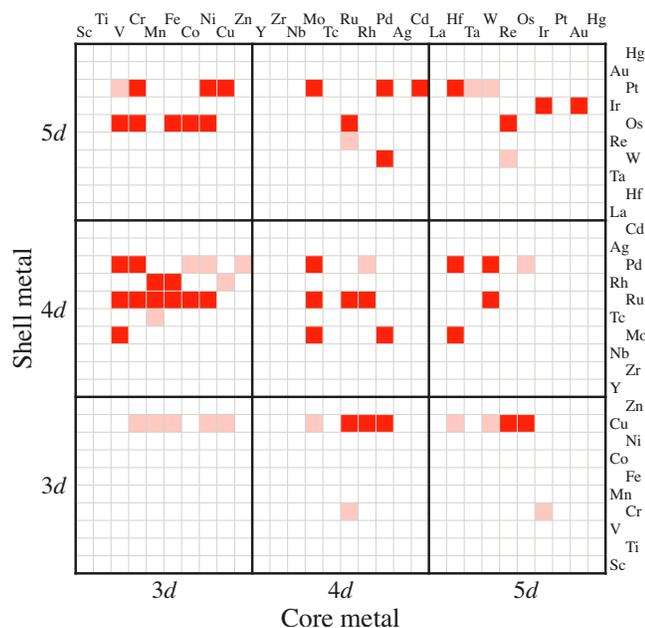
FIG. 6. Promising core-shell metal combinations for 38-atom particles revealed by the GA. Dark squares indicate particles that have $\Phi \leq 0.25$ eV; light squares have $\Phi \leq 0.50$ eV.

Fig. 6 indicates that the core is capable of influencing the electronic properties of the shell. Core metals with small lattice constants such as Cr, Mo, and V stand out. These cores induce compressive strain in the shell and transfer charge to the shell. Both of these effects contribute to a lowering of the surface d-band level, which tends to make the shell of the particle more noble.[34] These cores tend to increase catalytic activity by reducing the binding energy of oxygen.

B. Comparison of the GA to other search methods

To compare the effectiveness of the GA to other search methods, we examined all 900 core-shell metal combinations for 38-atom particles and performed a large number of GA, Monte Carlo (MC), and random sampling (RS) simulations. Simulations were run in sets of three so that the initial populations were the same for the methods. Overall, 300 simulations were performed, 100 for each method. Initial populations were chosen as outlined in Sec. II.

Generations of 30 nanoparticles were maintained in the MC and RS simulations; however, the processes by which particles were selected and created for new generations were different from the GA. In the RS simulation, each particle in the population was replaced with a new, random particle. In the MC simulation, a trial particle was generated for each particle in the population by performing a single-point mutation on the original particle (the trial particle therefore either had a different core or a different shell than the original particle; see Fig. 4). Trial particles were passed to the next generation according to the Metropolis acceptance probability[35]
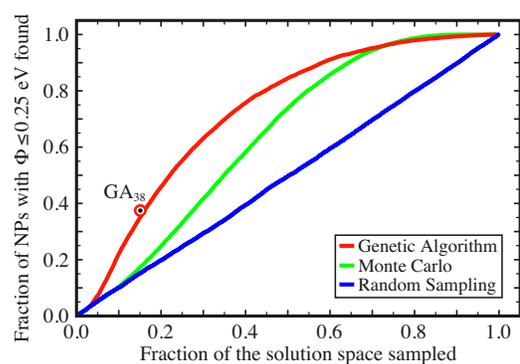
FIG. 7. Comparison of the GA, MC, and RS efficiencies. The fraction of particles with $\Phi \leq 0.25$ eV found is plotted against the fraction of the solution space sampled. The GA in Sec. III A (black dot) found more than twice as many fit particles as the other methods at that fraction of the solution space sampled.

$$P_{accept} = \min[1, e^{-(\Phi_{new} - \Phi_{old})/k_BT}], \qquad (3)$$

where k_BT is the effective thermal energy of the sampling, taken to be 0.25 eV, corresponding to an average acceptance probability of 17%.

The different optimization methods are compared in Fig. 7. For RS, the chance of finding a fit particle is constant and equal to their fraction of the solution space. The fraction of fit particles found with RS increases linearly with the fraction of the solution space sampled. Both the GA and MC methods outperform RS. Of the three methods, however, the GA found the fittest particles most efficiently. The GA in Sec. III A (represented by the black dot in Fig. 7) explored 15% of the solution space and found 37% of the fit particles; the MC and RS methods found only 17% and 15% of the fit particles, respectively, at this fraction of the solution space sampled. A comparison of the fit particles found in Sec. III A and the complete set found by brute force is shown in Fig. 8.
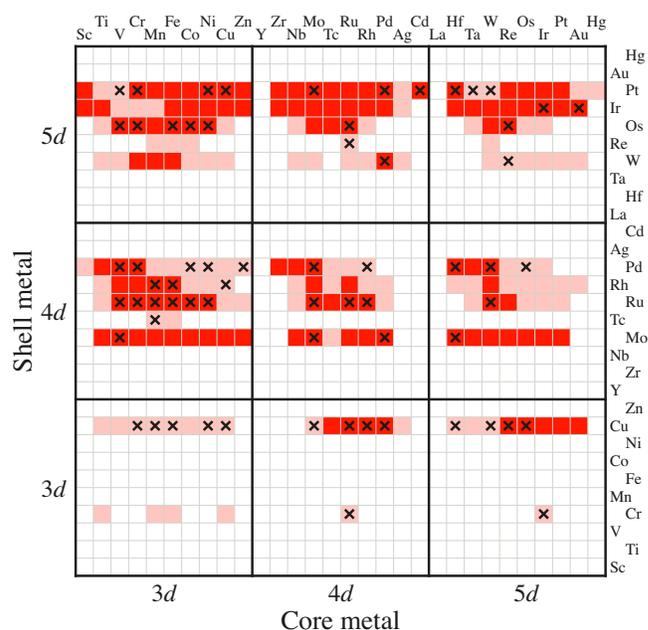
FIG. 8. Best 38-atom nanoparticles out of all 900 possible core-shell combinations. Dark and light squares are defined in Fig. 6. Squares with black X's represent the particles found by the GA in Sec. III A.
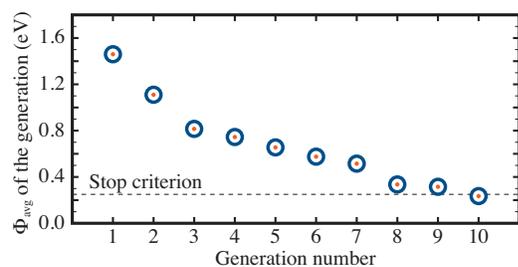
FIG. 9. Convergence of the 79-atom nanoparticle GA.

C. 79-atom nanoparticles

We have also applied the GA to larger, more realistic 79-atom core-shell nanoparticles. The convergence of the GA is shown in Fig. 9. Fit 79-atom particles found by the GA are shown in Fig. 10. Horizontal trends are again prominent, indicating that there may only be a few potential shell metals for use in 79-atom core-shell ORR catalysts. These metals are similar to those found for the 38-atom particles and include Cu, Ir, Os, Pd, Pt, Rh, and Ru.

Stability is an important concern for the small particles. In a few instances, core atoms were found to spontaneously migrate to the shell during structural minimization indicating that the particle was unstable. In the 79-atom GA, 35 of the 176 particles sampled (20%) did not meet our symmetry requirement, and were removed from the GA.

Several of the core-shell metal combinations in Figs. 8 and 10 have been investigated experimentally. Ni@Pt was among the very best of particles found by both the 38- and 79-atom GA. This combination of metals has been shown to be very effective for the ORR by Stamenkovic et al.[36] Ru@Pt has been shown by Alayoglu et al.[37] to be an effective catalyst for the ORR, as well as for CO oxidation in H$_2$-rich environments. Other examples include
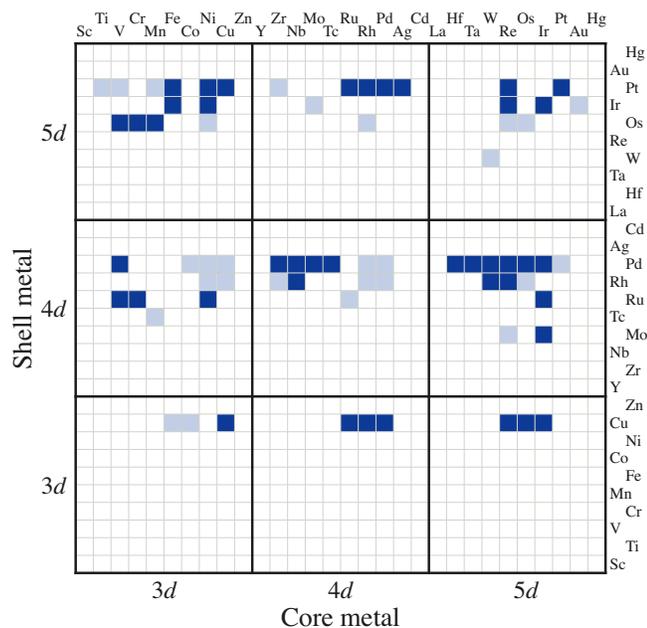
FIG. 10. Promising core-shell metal combinations for 79-atom particles revealed by the GA. Dark and light squares are defined in Fig. 6.
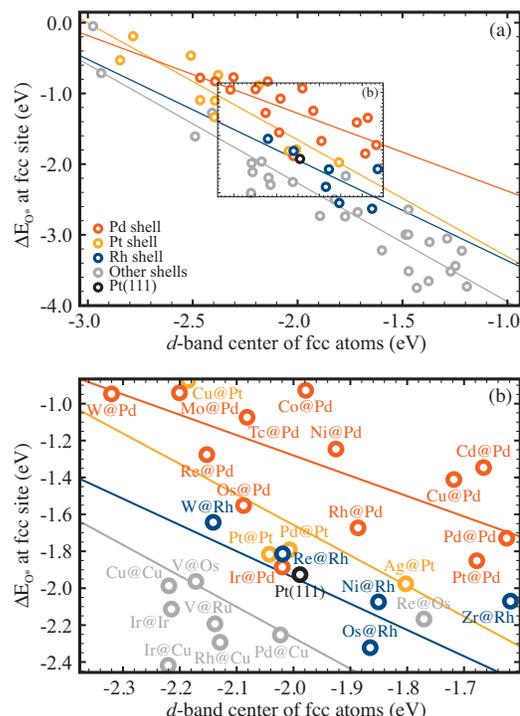
FIG. 11. Binding energy of atomic oxygen at a fcc site vs d-band level of the fcc atoms in the shell of 79-atom particles. The inset in (a) is shown in (b) on a larger scale.

Cu@Pt by Koh et al.,[38] Fe@Pd by Shao et al.,[39] and Co@Pd by Savadogo et al.[40] More candidates are shown in Figs. 8 and 10.

D. Oxygen binding on 79-atom particles

The energy level of the d-band is a good reactivity descriptor for catalytic activity, but there are other factors that determine adsorbate binding and reaction barriers; these energetics ultimately determine the reaction kinetics.[41,42] To further investigate the fittest 79-atom nanoparticle catalysts, we have calculated the binding energy of atomic oxygen to a fcc site on the (111) facet. The binding energy of oxygen species on transition metals has been shown to be important for the ORR and to correlate well with catalytic activity.[43,44] The (111) facet was chosen because it generally binds adsorbates weakest. Most particles investigated are less noble than Pt and bind oxygen too strongly, so the focus should be on weak binding sites. It is possible, however, that the (100) facet or the edge/corner sites on noble particles have suitable oxygen binding energies to be good catalysts. These sites are not identified here.

The relation between the oxygen binding energy and the d-band center is shown in Fig. 11. There is a linear correlation for particles with the same shell metal, yet there is considerable variation in the trend across different shell metals. This behavior is expected since there are other factors that affect adsorbate binding strength, such as the filling of the d-band and the overlap between adsorbate and surface metal orbitals. When these factors are constant (a good approximation when the shell metal is the same), a linear trend is observed.

To compare particles with different shell metals, the binding energy of oxygen is a better measure of catalytic activity than the *d*-band level. Metals with somewhat weaker oxygen binding than Pt are expected to have higher ORR activity.[24] An oxygen atom binds at a fcc hollow site on the Pt(111) surface with an energy of 1.93 eV relative to 1/2 $O_2(g)$ at 1/9 monolayer coverage.[33] Binding to the (111) facet of a 79-atom Pt particle is very similar, as can be seen in Fig. 11. In general, the binding energy decreases for reactive cores, e.g., W@Pd, Mo@Pd, and Co@Pd. These trends hold for other common shell metals, e.g., Pt and Rh.

If one knows the active site of the catalyst, the GA can be improved to more specifically target these kinetics. In our case, we used the average *d*-band level of the entire shell in our fitness function. If oxygen binding to a fcc site were known to be a more direct reactivity indicator, however, it would make sense to use the *d*-band level of the fcc atoms or even the oxygen binding energy itself. As long as these indicators are correlated [as in Fig. 11(a)], any one of them may be used to identify an optimal set of candidate catalysts. Subsequent refinements of our fittest nanoparticle catalysts with further calculations and experiments are needed to conclusively identify effective catalysts.

IV. DISCUSSION AND CONCLUSIONS

In this work, we used a GA to find core-shell nanoparticles with *d*-band centers close to that of Pt(111). For 38-atom particles, reactive metals such as V, Cr, and Mo were found to be good cores, while Cu, Ir, Mo, Os, Pd, Pt, Rh, and Ru were found to be good shells. For 79-atom particles, no core metals stood out, and Cu, Ir, Os, Pd, Pt, Rh, and Ru were found to be good shells. Calculations of the oxygen binding energy to the (111) facets of these particles showed a linear correlation with the *d*-band center for particles with the same shell, however, there was significant variation in the trend for different shells. Using the oxygen binding energy as a measure of catalytic activity, we were able to refine the set of fit nanoparticles identified by our GA and suggest new particles that can be tested experimentally.

GAs are only as good as their fitness function(s) allow them to be. In this work, particle fitness was based only on the *d*-band center of the shell, but other properties such as stability and metal cost are also important. Stability is particularly important for core-shell particles whose catalytic properties depend on the specific arrangement of the atoms. Including the surface-segregation energy of the particles in an oxidizing environment, for example, would be a good way to refine our calculations and identify stable particles. The GA could also be extended by using a more detailed genetic encoding, e.g., one that specifies the element identity of every atom in the particle instead of just the core and shell. This would vastly increase the number of candidate catalysts considered and extend their structures beyond the core-shell catalysts considered here. Variable-length chromosomes, moreover, could allow 38-atom particles to breed with 79-atom particles, the offspring of which could contain an intermediate number of atoms.

Promising platinum alternatives must be developed if fuel cells are to replace internal combustion engines as a future means of utilizing chemical energy. Feedback between experimentalists and theorists will likely play a critical role in determining whether such catalysts exist. Optimizing nanoparticles is easier to do computationally than experimentally. Experiments, however, will ultimately determine which catalysts are effective. Subsequent refining of our methods and models will make them more accurate and better able to identify effective catalysts in the future.

ACKNOWLEDGMENTS

[1] M. Haruta, T. Kobayashi, H. Sano, and N. Yamada, Chem. Lett. **2**, 405 (1987).

[2] M. Haruta, N. Yamada, T. Kobayashi, and S. Iijima, J. Catal. **115**, 301 (1989).

[3] F. Besenbacher, I. Chorkendorff, B. S. Clausen, B. Hammer, A. M. Molenbroek, J. K. Nørskov, and I. Stensgaard, Science **279**, 1913 (1998).

[4] J. Greeley and M. Mavrikakis, Nature Mater. **3**, 810 (2004).

[5] R. W. J. Scott, O. M. Wilson, S.-K. Oh, E. A. Kenik, and R. M. Crooks, J. Am. Chem. Soc. **126**, 15583 (2004).

[6] O. M. Wilson, R. W. J. Scott, J. C. Garcia-Martinez, and R. M. Crooks, J. Am. Chem. Soc. **127**, 1015 (2005).

[7] D. Levine, Comput. Oper. Res. **23**, 547 (1996).

[8] *Evolutionary Computation in Bioinformatics*, edited by G. B. Fogel and D. W. Corne (Academic, New York/Elsevier, New York, 2002).

[9] F. H. Van Batenburg and A. P. Gultyaev, J. Theor. Biol. **174**, 269 (1995).

[10] C. Gondro and B. P. Kinghorn, Genet. Mol. Res. **6**, 964 (2007).

[11] D. M. Deaven and K.-M. Ho, Phys. Rev. Lett. **75**, 288 (1995).

[12] M. Damsbo, B. S. Kinnear, M. R. Hartings, P. T. Ruhoff, M. F. Jarrold, and M. A. Ratner, Proc. Natl. Acad. Sci. U.S.A. **101**, 7215 (2004).

[13] P. Willett, Trends Biotechnol. **13**, 516 (1995).

[14] O. Cordón, F. Herrera, and L. Sánchez, in *Genetic Algorithms and Evolution Strategy in Engineering and Computer Science*, edited by D. Quagliarella, J. Périaux, C. Poloni, and G. Winter (Wiley, New York, 1998), pp. 205–224.

[15] M. A. Falcone, H. S. Lopes, and L. D. S. Coelho, Int. J. Comput. Appl. Technol. **31**, 158 (2008).

[16] J. R. Koza, in *Economics and Cognitive Science*, edited by P. Bourgine and B. Walliser (Pergamon, New York, 1991), pp. 57–75.

[17] J.-Y. Potvin, P. Soriano, and M. Vallée, Comput. Oper. Res. **31**, 1033 (2004).

[18] D. Yuret and M. Maza, Technical Analysis of Stocks & Commodities **12**, 58 (1994).

[19] G. H. Jóhannesson, T. Bligaard, A. V. Ruban, H. L. Skriver, K. W. Jacobsen, and J. K. Nørskov, Phys. Rev. Lett. **88**, 255506 (2002).

[20] S. A. Vinterbo and L. Ohno-Machado, Artif. Intell. Med. **18**, 117 (2000).

[21] R. Smigrodzki, B. Goertzel, C. Pennachin, L. Coelho, F. Prosdocimi, and W. D. Parker, Jr., Artif. Intell. Med. **35**, 227 (2005).

[22] J. Greeley, J. K. Nørskov, and M. Mavrikakis, Annu. Rev. Phys. Chem. **53**, 319 (2002).

[23] T. Bligaard, J. K. Nørskov, S. Dahl, J. Matthiesen, C. H. Christensen, and J. Sehested, J. Catal. **224**, 206 (2004).

[24] J. K. Nørskov, J. Rossmeisl, A. Logadottir, L. Lindqvist, J. R. Kitchin, T. Bligaard, and H. Jónsson, J. Phys. Chem. B **108**, 17886 (2004).

[25] Y. Wang, S. Curtarolo, C. Jiang, R. Arroyave, T. Wang, G. Ceder, L.-Q. Chen, and Z.-K. Liu, Calphad: Comput. Coupling Phase Diagrams Thermochem. **28**, 79 (2004).

[26] G. Kresse, Phys. Rev. B **62**, 8295 (2000).

[27] G. Kresse and J. Hafner, Surf. Sci. **459**, 287 (2000).

[28] P. E. Blöchl, Phys. Rev. B **50**, 17953 (1994).

[29] G. Kresse and J. Joubert, Phys. Rev. B **59**, 1758 (1999).

[30] G. Kresse and J. Furthmüller, Comput. Mater. Sci. **6**, 15 (1996).

[31] J. P. Perdew and Y. Wang, Phys. Rev. B **45**, 13244 (1992).

[32] M. Methfessel and A. T. Paxton, Phys. Rev. B **40**, 3616 (1989).

[33] A six-layer $p(3 \times 3)$ Pt slab was used to calculate the d-band level of Pt(111) and the binding energy of O at a fcc site on Pt(111). These calculations used the same DFT parameters as the nanoparticles, except that the Brillouin zone was sampled with a $9 \times 9 \times 1$ Monkhorst–Pack k-point mesh.

[34] L. Calderín, L. E. González, and D. J. González, J. Chem. Phys. **130**, 194505 (2009).

[35] N. Metropolis, A. W. Rosenbluth, M. N. Rosenbluth, A. H. Teller, and E. Teller, J. Chem. Phys. **21**, 1087 (1953).

[36] V. R. Stamenkovic, B. Fowler, B. S. Mun, G. Wang, P. N. Ross, C. A. Lucas, and N. M. Marković, Science **315**, 493 (2007).

[37] S. Alayoglu, A. U. Nilekar, M. Mavrikakis, and B. Eichhorn, Nature Mater. **7**, 333 (2008).

[38] S. Koh and P. Strasser, J. Am. Chem. Soc. **129**, 12624 (2007).

[39] M. H. Shao, K. Sasaki, and R. Adzic, J. Am. Chem. Soc. **128**, 3526 (2006).

[40] O. Savadogo, K. Lee, K. Oishi, S. Mitsushima, N. Kamiya, and K.-I. Ota, Electrochem. Commun. **6**, 105 (2004).

[41] B. Hammer, L. B. Hansen, and J. K. Nørskov, Phys. Rev. B **59**, 7413 (1999).

[42] B. Hammer and J. K. Nørskov, Adv. Catal. **45**, 71 (2000).

[43] J. K. Nørskov, T. Bligaard, A. Logadottir, S. Bahn, L. B. Hansen, M. Bollinger, H. Bengaard, B. Hammer, Z. Sljivancanin, M. Mavrikakis, Y. Xu, S. Dahl, and C. J. H. Jacobsen, J. Catal. **209**, 275 (2002).

[44] A. U. Nilekar, Y. Yu, J. Zhang, M. B. Vukmirovic, K. Sasaki, R. R. Adzic, and M. Mavrikakis, Top. Catal. **46**, 276 (2007).